SYNTHESIS AND PROPERTIES
OF INORGANIC COMPOUNDS

Phase Formation, Crystal Structure, and Electrical Conductivity of Triple Phosphates of Alkali Metals and Titanium

E. A. Asabina[a], V. I. Pet'kov[a], M. V. Boguslavskii[b], A. P. Malakho[b], and B. I. Lazoryak[b]

[a] *Nizhni Novgorod State University, pr. Gagarina 23, Nizhni Novgorod, 603950 Russia*
[b] *Moscow State University, Vorob'evy gory, Moscow, 119992 Russia*

Received January 26, 2006

Abstract—For triple phosphates of composition $A_{0.5}A'_{0.5}Ti_2(PO_4)_3$ (A–A' = Li–Na, Na–K, K–Rb), phase formation is studied, the crystal structure is refined, and the electrical conductivity is measured. The compounds are classified with the $NaZr_2(PO_4)_3$ structure type (NZP, space group $R\bar{3}c$). The phosphate frameworks are built of TiO_6 octahedra and PO_4 tetrahedra. Extraframework positions M1 are fully occupied by randomly distributed alkali cations. Positions M2 are vacant. Correlations are found between the structural distortion and electrical conductivity of the phosphates, on one hand, and the alkali cation size, on the other.

Double alkali metal phosphates of Group IVB elements of the composition $AD_2(PO_4)_3$ (A = Li, Na, K, Rb, Cs; D = Ti, Zr, Hf) are now known (Table 1). Many of them are structurally studied. Their main structural feature is a stable framework built of DO_6 octahedra and PO_4 tetrahedra; alkali metal atoms populate the interstices in the framework. Such phosphates are of interest because of their high chemical and thermal stability, radiation-damage stability, and several other valuable physical and chemical properties [17]. In particular, compounds with the $NaZr_2(PO_4)_3$-type structure (NZP, NASICON) containing small extraframework cations (Li^+, Na^+) frequently have high ionic conductivity [18–20].

The NZP structure is distinguished by its high isomorphic capacity for different types of cations with different sizes and oxidation numbers: cations, either individually or in combinations, can occupy the framework and extraframework positions. Phase formation in $A_{1-x}A'_xD_2(PO_4)_3$ (D = Ti, Zr) system was studied in [21, 22]; the concentration and temperature limits of stability for the NZP structure were determined. The investigations of mixed-alkali triple phosphates have been confined to X-ray diffraction experiments; the alkali cation distribution in the crystal lattice remains unclear. The structural studies of such phosphates are of theoretical interest: they would help to understand the isovalent isomorphism features in framework compounds with the lattice symmetry being conserved. They are also of applied interest for developing engineering ceramics.

The goal of this work is to synthesize triple phosphates $A_{0.5}A'_{0.5}Ti_2(PO_4)_3$ (A–A' = Li–Na, Na–K, K–Rb); to refine their crystal structures on the basis of powder data (the Rietveld method); to discuss how cationic substitutions influence the structural features of phosphates with similar chemical formulas, structural parameters, and symmetry; and to study the electrical conductivity of ceramic samples of the triple phosphates from 298 to 1223 K.

EXPERIMENTAL

The starting chemicals used in the synthesis of $A_{0.5}A'_{0.5}Ti_2(PO_4)_3$ (A–A' = Li–Na, Na–K, K–Rb) triple phosphates were aqueous solutions of high-purity reagents (Li_2CO_3, NaCl, KCl, RbCl, $NH_4H_2PO_4$) and a $TiOCl_2$ solution prepared by oxidizing $TiCl_3$ with a mixture of nitric and hydrochloric acids. The synthesis procedure was as follows. Stoichiometric amounts of the aqueous solutions of alkali metal chlorides and titanium oxychloride were combined at room temperature under continuous stirring; then, an ammonium dihydrogen phosphate solution was added under stirring also in accordance with the stoichiometry. The resulting gel was dried at 353 K and, then, heat-treated with free access to air at 873–1473 K. Since minor crystalline phases with a low diffusion mobility can form upon rapid temperature elevation, the annealing temperature was consecutively elevated in 100-K steps; the annealing duration was 24–30 h with additional dispersion at each step.

Control over the chemical composition and homogeneity of the samples wad performed using a Cam-

ASABINA et al.

Table 1. Crystal data for alkali metal phosphates of Group IVB elements (A = Li, Na, K, Rb, Cs; D = Ti, Zr, Hf)

| Compound	Space group	Unit cell parameters					Source
		a, Å	b, Å	c, Å	α, β, γ, deg	V, Å^3	
LiTi$_2$(PO$_4$)$_3^*$	$R\bar{3}c$	8.51173(4)		20.8524(2)		1308.35	[1]
NaTi$_2$(PO$_4$)$_3^*$	$R\bar{3}c$	8.4502(5)		21.833(9)		1366.74	[2]
	$R\bar{3}c$	8.4854(2)		21.7994(8)		1359.33	[3]
KTi$_2$(PO$_4$)$_3^*$	$R\bar{3}c$	8.367(1)		23.074(3)		1398.9	[4]
RbTi$_2$(PO$_4$)$_3^*$	$R\bar{3}c$	8.290(1)		23.530(4)		1400.3	[5]
LiZr$_2$(PO$_4$)$_3^*$	$R\bar{3}c$ (423 K)	8.85493(3)		22.1440(1)		1503.69	[6]
	$C\bar{1}$	15.0718(2)	8.8556(1)	9.1234(1)	$\alpha = 89.660(1)$ $\beta = 123.912(1)$ $\gamma = 90.429(1)$	1010.52	[7]
	$P2_1/n$	8.81277(4)	8.94520(5)	12.37540(6)	90.801(1)	975.482	[8]
	$Pbna$ (623 K)	8.84303(5)	8.94120(6)	12.41301(8)		981.463	[8]
NaZr$_2$(PO$_4$)$_3^*$	$R\bar{3}c$	8.815(1)		22.746(7)		1530.7	[9]
KZr$_2$(PO$_4$)$_3^*$	$R\bar{3}c$	8.71(1)		23.89(2)		1569.6	[10]
RbZr$_2$(PO$_4$)$_3$	$R\bar{3}c$	8.66(1)		24.38(2)		1583.4	[11]
CsZr$_2$(PO$_4$)$_3^*$	$R\bar{3}c$	8.5758(2)		24.9061(4)		1586.30	[12]
LiHf$_2$(PO$_4$)$_3^*$	$R\bar{3}c$ (320 K)	8.83070(6)		22.0272(2)		1487.58	[13]
	$P\bar{1}$ (175 K)	8.69447(8)	8.74104(7)	9.07206(7)	$\alpha = 118.6297(6)$ $\beta = 90.6805(8)$ $\gamma = 119.1605(7)$	500.663	[13]
NaHf$_2$(PO$_4$)$_3$	$R\bar{3}c$	8.7707(5)		22.66(2)		1509.7	[14]
KHf$_2$(PO$_4$)$_3^*$	$R\bar{3}c$	8.6819(4)		23.862(2)		1557.64	[15]
RbHf$_2$(PO$_4$)$_3$	$R\bar{3}c$	8.63(1)		24.34(2)		1569.9	[16]
CsHf$_2$(PO$_4$)$_3$	$R\bar{3}c$	8.54(1)		24.81(2)		1567.0	[16]

* The crystal structure has been solved.

Scan MV 2300 scanning electron microscope equipped with a Link Inca Energy 200C energy-dispersive detector. The PAP correction procedure was used in composition calculations. The error of the composition determinations was within 2.5 wt %.

The X-ray diffraction data were collected at room temperature on a Thermo ARL X'tra powder diffractometer (CuK_α radiation, reflection geometry, Peltier semiconductor detector). X-ray powder diffraction was used to determine the phase composition of the samples during their synthesis after each isothermal annealing step and to control the single-phase composition of the resulting compounds. The 2θ range was 10°–60°. In

structure solution experiments, X-ray diffraction patterns were measured in the range 2θ = 5°–110° in 0.02° steps. The X-ray diffraction patterns were processed and the structure was refined by the Rietveld method [23] using RIETAN97 software [24]. The peak profiles were described by a modified pseudo-Voigt function (Mod-TCH pV [25]).

Second harmonic generation (SHG) signals were measured in fine-grained powders on a high-sensitivity two-channel setup using the procedure described in [26]. The radiation source used was a Q-switched pulsed laser with a wavelength of 1.064 μm. The reference used was crystalline α-quartz powdered to a grain
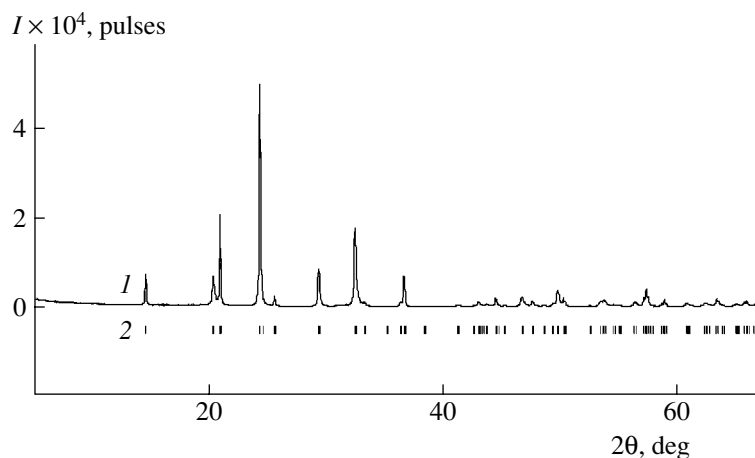
Fig. 1. Fragments of (*1*) the observed X-ray diffraction pattern and (*2*) the stick diagram for $Li_{0.5}Na_{0.5}Ti_2(PO_4)_3$.
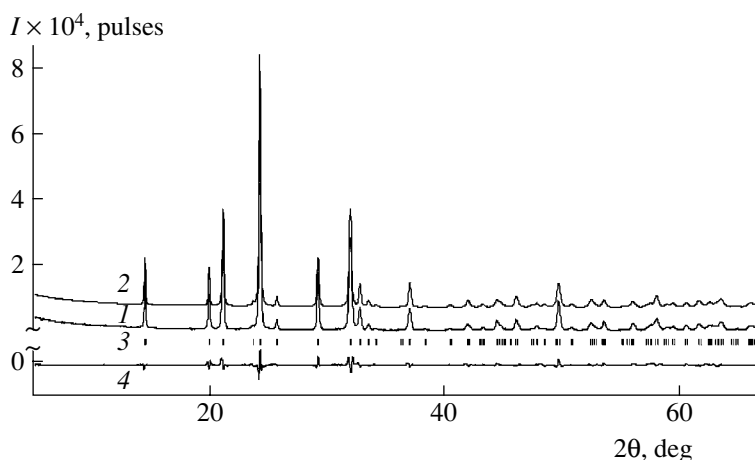
Fig. 2. Fragments of (*1*) observed, (*2*) simulated, and (*4*) difference X-ray diffraction patterns and (*3*) the stick diagram for $Na_{0.5}K_{0.5}Ti_2(PO_4)_3$. The simulated pattern is shifted relative to the observed pattern.

size of 3–5 μm. The SHG signals generated in the test sample and reference were recorded in reflection geometry.

The ceramics for electrical conductivity measurements shaped as disks 8 mm in diameter and 1–2 mm height were manufactured by sintering at 1373 K for 6 h of a powder compacted at ~500 MPa.

Platinum electrodes were applied to the end surfaces of the disks by burning-in colloidal platinum. The conductivity was measured with a two-point probe using an R-5083 ac bridge at frequencies from 1 Hz to 100 kHz and an E7-12 ac bridge at 1 MHz. The bridges were operated and data were processed with a computer.

RESULTS AND DISCUSSION

Synthesis and characterization. X-ray powder diffraction shows complex interactions between the components in the reaction mixtures. Reflections of titanium pyrophosphate were in the X-ray diffraction patterns of the samples annealed at 873 K. Crystalline

titanium pyrophosphate is an intermediate; it fully converts into triple phosphates of titanium and alkali metals only when the temperature is stepwise elevated further. Single-phase $A_{0.5}A'_{0.5}Ti_2(PO_4)_3$ products are formed at 1073–1173 K. After annealing at 1473 K for 6 h, the samples partially decompose. Reflections from titanium dioxide are observed in the X-ray diffraction patterns of samples annealed at 1473 K. Other decomposition products are likely alkali phosphates.

$A_{0.5}A'_{0.5}Ti_2(PO_4)_3$ crystals for the structural experiments and electrical conductivity measurements were obtained at 1273 K. X-ray powder diffraction shows that the phosphates belong to the NZP type. Microprobe measurements show that the samples are homogeneous and their compositions are close to those calculated for the $A_{0.5}A'_{0.5}Ti_2(PO_4)_3$ formula.

Structures of $A_{0.5}A'_{0.5}Ti_2(PO_4)_3$ phosphates. The choice of space group $R\bar{3}c$ for the $A_{0.5}A'_{0.5}Ti_2(PO_4)_3$

Table 2. Details of the X-ray diffraction experiment and the results of structure refinement for $A_{0.5}A'_{0.5}Ti_2(PO_4)_3$ phosphates

Compound	$Na_{0.5}K_{0.5}Ti_2(PO_4)_3$	$K_{0.5}Rb_{0.5}Ti_2(PO_4)_3$
Space group	$R\bar{3}c$ (No. 167)	
Z	6	
2θ range, deg	5–110	
Unit cell parameters:		
a, Å	8.4129(3)	8.3300(1)
c, Å	22.5426(8)	23.2723(3)
V, Å^3	1381.74(9)	1398.49(3)
Number of reflections	195	199
Number of refined parameters*	18 + 13	16 + 13
Final values, %**		
R_{wp}; R_p	8.37; 6.20	7.18; 5.01
R_I; R_F	2.45; 0.98	3.30; 1.97
S	3.36	2.41

Notes: * The first figure includes the background and profile parameters, scaling factor, and unit cell parameters; the second figure includes the positional and thermal parameters of atoms and site occupancies.
** Calculated using formulas from [25].

Table 3. Coordinates and isotropic thermal parameters of atoms in the structures of $Na_{0.5}K_{0.5}Ti_2(PO_4)_3$ (**I**) and $K_{0.5}Rb_{0.5}Ti_2(PO_4)_3$ (**II**)

Compound	Atom	Position	x	y	z	B, Å^2
I	A(A')	6b	0	0	0	3.12(1)
II			0	0	0	3.63(6)
I	Ti	12c	0	0	0.1479(1)	0.46(5)
II			0	0	0.1505(1)	0.37(4)
I	P	18e	0.7156(2)	0	0.25	1.17(6)
II			0.7184(2)	0	0.25	0.92(5)
I	O1	36f	0.2020(4)	0.1589(3)	0.3065(1)	0.89(9)
II			0.2085(4)	0.1500(3)	0.3020(1)	0.43(8)
I	O2	36f	0.4753(4)	0.3014(4)	0.2387(1)	1.41(9)
II			0.4700(4)	0.3032(4)	0.2330(1)	0.99(8)

triple phosphates (A–A' = Li–Na, Na–K, K–Rb) is confirmed by SHG measurements in fine-grained powders. The absence of an SHG signal for all samples proves their centrosymmetry.

Figure 1 displays the X-ray diffraction results obtained in the angle range 5°–110° with 0.02° steps for $Li_{0.5}Na_{0.5}Ti_2(PO_4)_3$. This triple phosphate sample is a single phase; it has the NZP-type structure, and its X-ray powder diffraction pattern is indexed in terms of space group $R\bar{3}c$. For $LiTi_2(PO_4)_3$, neutron diffraction showed lithium cation disorder in interstices [1]. However, X-ray powder diffraction data for $Li_{0.5}Na_{0.5}Ti_2(PO_4)_3$ do not reveal the distribution character of the alkali cations in the framework interstices. The following unit cell parameters were calculated for $Li_{0.5}Na_{0.5}Ti_2(PO_4)_3$: $a = 8.4871(9)$ Å, $c = 21.752(2)$ Å, $V = 1356.9(2)$ Å^3.

$I \times 10^4$, pulses
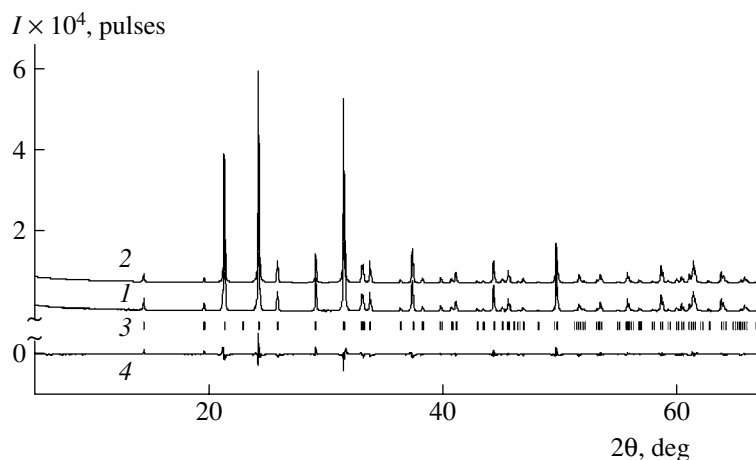
Fig. 3. Fragments of (*1*) observed, (*2*) simulated, and (*4*) difference X-ray diffraction patterns and (*3*) the stick diagram for $K_{0.5}Rb_{0.5}Ti_2(PO_4)_3$. The simulated pattern is shifted relative to the observed pattern.

The starting models used in the structure refinement for the $A_{0.5}A'_{0.5}Ti_2(PO_4)_3$ (A–A' = Na–K, K–Rb) compounds were the atomic coordinates in the structures of titanium alkali phosphates $ATi_2(PO_4)_3$, where A = Na or K (space group $R\bar{3}c$) [3, 4]. Table 2 displays the details of the X-ray diffraction experiment and structure refinement. Figures 2 and 3 show the observed, simu-

lated, stick, and difference X-ray diffraction patterns for the $A_{0.5}A'_{0.5}Ti_2(PO_4)_3$ phosphates.

There is good fit between the observed and simulated X-ray diffraction patterns for $Na_{0.5}K_{0.5}Ti_2(PO_4)_3$ and $K_{0.5}Rb_{0.5}Ti_2(PO_4)_3$ (Figs. 2, 3). The unit cell parameters and the final refinement values for these phosphates are listed in Table 2. The coordinates of atoms

Table 4. Selected interatomic distances and bond angles in TiO_6 and PO_4 polyhedra in the structures of $Na_{0.5}K_{0.5}Ti_2(PO_4)_3$ (**I**) and $K_{0.5}Rb_{0.5}Ti_2(PO_4)_3$ (**II**)

Compound	Bond	d, Å	Compound	Angle	ω, deg
I	A(A')–O2 (×6)	2.604(3)	**I**	O1PO1'	112.7(3)
II		2.790(3)	**II**		110.7(2)
I	Ti–O1 (×3)	1.859(3)	**I**	O1PO2 (×2)	106.3(2)
II		1.905(3)	**II**		107.6(1)
I	Ti–O2 (×3)	1.917(3)	**I**	O1PO2 (×2)	109.9(2)
II		1.923(3)	**II**		109.1(1)
I	P–O1 (×2)	1.577(3)	**I**	O2PO2'	111.8(3)
II		1.539(3)	**II**		112.8(3)
I	P–O2 (×2)	1.560(3)	**I**	O1TiO1' (×3)	92.5(2)
II		1.540(3)	**II**		89.7(1)
			I	O1TiO2 (×3)	89.7(1)
			II		87.5(1)
			I	O1TiO2 (×3)	92.8(1)
			II		96.1(1)
			I	O1TiO2 (×3)	174.3(2)
			II		173.6(1)
			I	O2TiO2' (×3)	84.9(1)
			II		87.0(1)

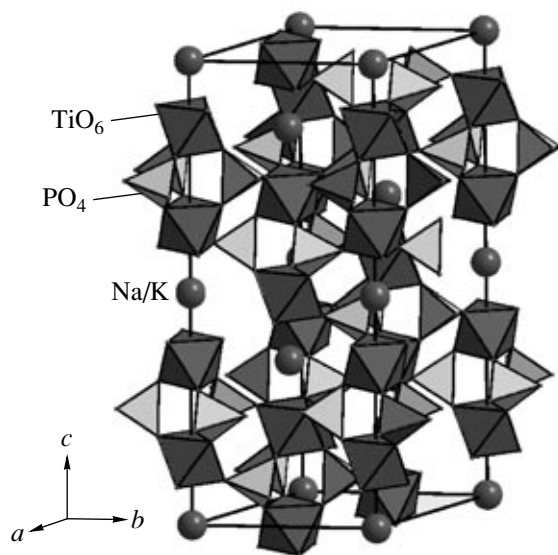**Fig. 4.** Fragment of the structure of $Na_{0.5}K_{0.5}Ti_2(PO_4)_3$.

and their isotropic thermal parameters are listed in Table 3. Selected interatomic distances and bond angles are listed in Table 4.

Figure 4 shows the $Na_{0.5}K_{0.5}Ti_2(PO_4)_3$ structure as an example of a test sample. The basis of the structure is a mixed 3D framework built of corner-sharing TiO_6 octahedra and PO_4 tetrahedra. Each octahedron is linked to six tetrahedra, and each tetrahedron is linked to four octahedra. The main building elements of the framework are fragments composed of two octahedra and three tetrahedra; these fragments form columns running along axis c. The columns are linked with each other through shared PO_4 tetrahedra. The alkali cations in the $A_{0.5}A'_{0.5}Ti_2(PO_4)_3$ compounds are randomly distributed in the fully occupied interstitial octahedral positions M1 inside the columns. The refinement of the occupancies of the M2 interstices between the columns for the alkali cations shows that these positions are vacant.

The unit cell parameters are monotone functions of alkali cation size in both the $ATi_2(PO_4)_3$ double phosphates and the $A_{0.5}A'_{0.5}Ti_2(PO_4)_3$ triple phosphates (Fig. 5). For the mixed-alkali triple phosphates, the unit cell parameters are additive relative to the unit cell parameters of the double phosphates; that is, in these compounds there is a mean radius of the formal alkali cation in the interstices: $r(A_{0.5}A'_{0.5}) = 0.5[r(A) + r(A')]$. The systematic increase in the parameter c and the decrease in the parameter a in response to the increasing alkali cation radius are due to the distortion of the columns built of TiO_6 octahedra and PO_4 tetrahedra; this distortion is a result of a correlated turn of the fragments of the framework upon the entrance of larger cat-
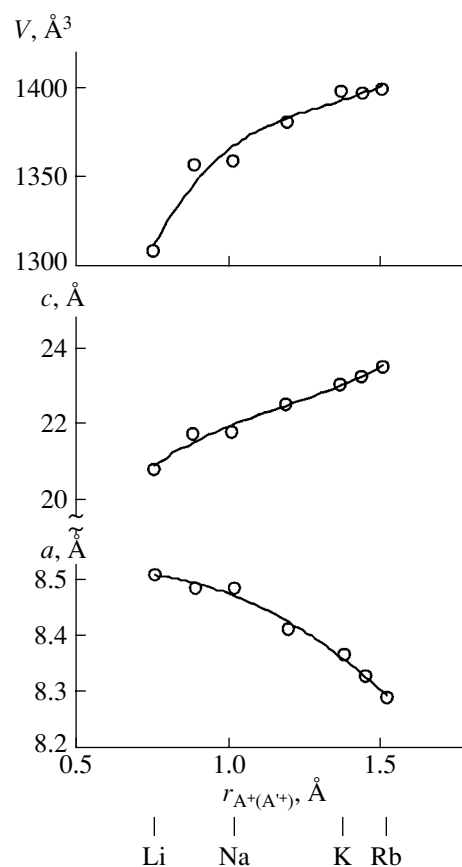

Fig. 5. Plots of the unit cell parameters a, c, and V vs. alkali cation radius in $ATi_2(PO_4)_3$ double phosphates and $A_{0.5}A'_{0.5}Ti_2(PO_4)_3$ triple phosphates.

ions into the M1 interstices (Fig. 6). The data displayed in Table 4 confirm the correlation between the structure distortion and the A and A' cation sizes: the bond lengths in the TiO_6 octahedra systematically increase, the bond lengths in the PO_4 tetrahedra decrease, and the OTiO and OPO bond angles change as the mean radius of the extraframework alkali cation increases.

The A(A')–O bond length for the phosphates in question is a linear function of the mean alkali cation size (Fig. 7). From an analysis of the interatomic distances in NZP phosphates of titanium and alkali metals, it is evident that the framework cation–oxygen bond lengths (Ti–O, P–O) are only weakly affected by the extraframework cation radius. This weak effect is due to the fact that the covalent chemical bonds in the framework are far stronger than the bonds formed by the extraframework cations.

Our data and previous data obtained in [1–6, 9, 10, 12, 13, 15] show that a $\{[L_2(XO_4)_3]^{p-}\}_{3\infty}$ three-dimensional framework is the base of the NZP-type structures; here, L is the structure-forming octahedral cation with the dominance of the metal–oxygen bond covalence, X is the anion-forming element with a tetrahedral rosette of chemical bonds, and p is the framework
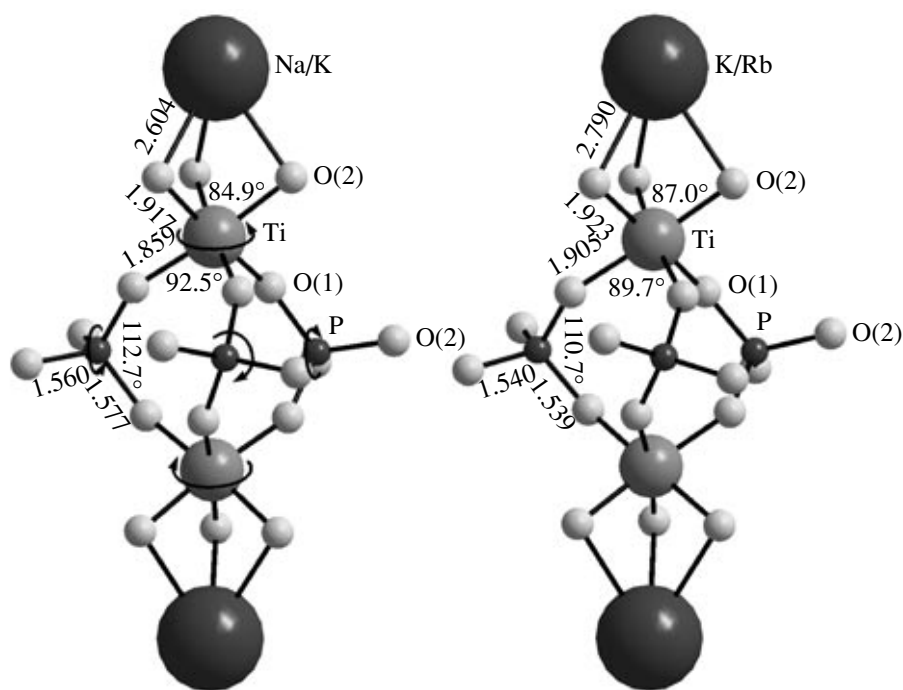
Fig. 6. Distortion of the framework structural fragments as a function of the alkali cation radius in the extraframework positions M1.

charge. Phosphorus is the anion-forming element in most of the NZP compounds. Similar frameworks are encountered in other classes of compounds that belong to the structural types of scandium tungstate $Sc_2(WO_4)_3$, langbeinite $K_2Mg_2(SO_4)_3$, and garnet $Ca_3Al_2(SiO_4)_3$. The crystal-chemical analysis of the $\{[L_2(XO_4)_3]^{p-}\}_{3\infty}$ framework for these four structural types is carried out in [27, 28].

Cation mobility in phosphates. The electrical conductivity of the $A_{0.5}A'_{0.5}Ti_2(PO_4)_3$ (A–A' = Li–Na, Na–K, K–Rb) ceramic samples was measured from room temperature to 1223 K. Electrical conductivity versus temperature curves are displayed in Fig. 8. The $\log(\sigma T)$–$(10^3/T)$ plots for the phosphates are linear; that is, the conductivity increases with temperature in accordance with the law

$$\sigma T = \sigma_0 \exp(-E_\sigma/kT),$$

where E_σ is the activation energy of conductivity, and σ_0 is the frequency factor. The conductivities at 1223 K and activation energies are listed in Table 5.

The characteristic feature of the NZP compounds is the geometric possibility of cation exchange between the extraframework positions [18, 19]. The interstices account for a significant volume of the framework; they penetrate the NZP framework, creating favorable conditions for ionic conductivity. Inasmuch as the temperature behavior of the electrical conductivity is similar

and the crystal-chemical reasons for the conductivity are the same both in previously known NZP phosphates and in those studied here, there is good reason to think that the origin of the conductivity in all NZP compounds is the same: the conductivity is due to the alkali cation mobility. The lower electrical conductivity of the $A_{0.5}A'_{0.5}Ti_2(PO_4)_3$ phosphates compared to the classical NASICON ionic conductors [18] is likely due to the low concentration of mobile ions in the interstices and the smaller interstice sizes in the titanium-containing framework than in the zirconium compounds.
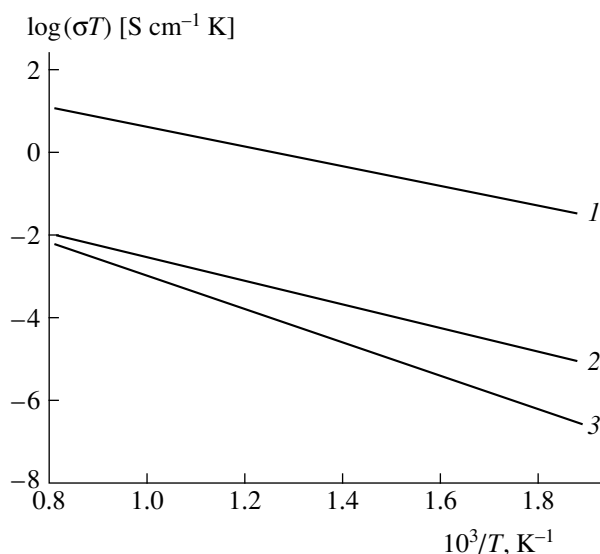
The electrical conductivity of the $A_{0.5}A'_{0.5}Ti_2(PO_4)_3$ phosphates is significantly affected by the A and A' alkali cation sizes. The highest σ over a wide temperature range is observed for $Li_{0.5}Na_{0.5}Ti_2(PO_4)_3$ (Fig. 8). Ion transport through the crystal structure of this phosphate is the least hindered, which follows from the comparison of the activation energies listed in Table 5.

Table 5. Electrical conductivity and activation energy in $A_{0.5}A'_{0.5}Ti_2(PO_4)_3$ (A–A' = Li–Na, Na–K, K–Rb) phosphates

Compound	$\sigma_{1223\ K}$, S/cm	E_σ, eV
$Li_{0.5}Na_{0.5}Ti_2(PO_4)_3$	8.6×10^{-3}	0.47
$Na_{0.5}K_{0.5}Ti_2(PO_4)_3$	7.1×10^{-6}	0.56
$K_{0.5}Rb_{0.5}Ti_2(PO_4)_3$	4.5×10^{-6}	0.80
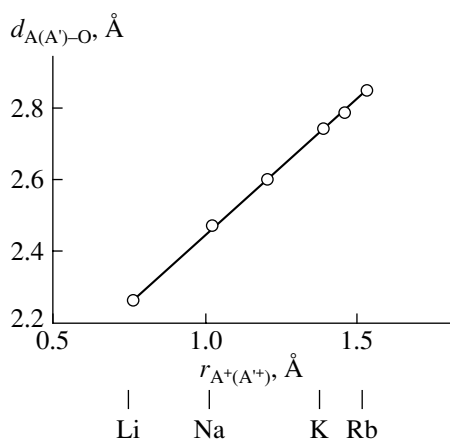
Fig. 7. A(A')–O bond length vs. alkali cation radius in $ATi_2(PO_4)_3$ double phosphates and $A_{0.5}A'_{0.5}Ti_2(PO_4)_3$ triple phosphates.

Fig. 8. Electrical conductivity (at 10 kHz) vs. temperature in $A_{0.5}A'_{0.5}Ti_2(PO_4)_3$ phosphates: A–A' = (*1*) Li–Na, (*2*) Na–K, and (*3*) K–Rb.

The increasing mean cation radius in the extraframework positions decreases the cation mobility in the interstices and, accordingly, decreases σ and increases E_σ, in correlation with the cationic conductivity model for the compounds in question.

To summarize, we have fulfilled systematic investigations of the $A_{0.5}A'_{0.5}Ti_2(PO_4)_3$ (A–A' = Li–Na, Na–K, K–Rb) triple phosphates, including their synthesis, structure refinement, and electrical conductivity measurements as a function of temperature. These phosphates crystallize within the temperature range from 1173 to 1423 K. They have the NZP-type structure; their frameworks are built of TiO_6 octahedra and PO_4 tetrahedra, and the alkali metal cations are randomly distributed in extraframework positions M1. Crystalchemical analysis and comparison with other phosphates show their structural relations to the NASICON ionic conductor. Correlations are found between the structural distortion, unit cell parameters, and electrical conductivity of the phosphates, on one hand, and the A and A' alkali cation sizes, on the other. By analogy with the known NZP phases, the electrical conductivity in the new triple phosphates is explained by the mobility of the alkali cations in the interstices.

ACKNOWLEDGMENTS

REFERENCES

1. D. A. Woodcock and P. Lightfoot, J. Mater. Chem. **9** (11), 2907 (1999).
2. Yu. A. Ivanov, E. L. Belokoneva, Yu. K. Egorov-Tismenko, et al., Dokl. Akad. Nauk SSSR **252** (5), 1122 (1980).
3. J. L. Rodrigo, P. Carrasco, and J. Alamo, Mater. Res. Bull. **24**, 611 (1989).
4. E. S. Lunezheva, B. A. Maksimov, and O. K. Mel'nikov, Kristallografiya **34**, 1119 (1989).
5. R. Duhlev, Acta Crystallogr., Sect. C: Cryst. Struct. Commun. **50**, 1525 (1994).
6. M. Catti and S. Stramare, Solid State Ionics **136–137**, 489 (2000).
7. M. Catti, S. Stramare, and R. Ibberson, Solid State Ionics **123**, 173 (1999).
8. M. Catti, N. Mortante, and R. M. Ibberson, J. Solid State Chem. **152**, 340 (2000).
9. H. Y.-P, Hong, Mater. Res. Bull. **11** (2), 173 (1976).
10. M. Sljukic, B. Matkovic, B. Prodic, and D. Anderson, Z. Kristallogr.: Kristallogeom., Kristallophys., Kristallochem. **130**, 148 (1969).
11. M. Šljukić, B. Matković, B. Prodić, and S. Šcavnicar, Croatica Chem. Acta **39**, 145 (1967).
12. E. R. Gobechiya, Yu. K. Kabalov, V. I. Pet'kov, and M. V. Sukhanov, Kristallografiya **49** (5), 829 (2004) [Crystallogr. Rep. **49** (5), (2004)].
13. E. Morin, T. Le Mercier, M. Quarton, et al., Powder Diffr. **14** (1), 53 (1999).
14. B. E. Taylor, A. D. English, and T. Berzins, Mater. Res. Bull. **12** (2), 171 (1977).
15. H. McMurdie, M. Morris, E. Evans, et al., Powder Diffr. **2** (1), 50 (1987).
16. B. Matković, B. Prodić, and M. Šljukić, Bull. Soc. Chem. Fr., No. 4, 1777 (1968).
17. V. I. Pet'kov and E. A. Asabina, Steklo Keram., No. 7, 23 (2004) [Glass Ceram., No. 7-8, 223 (2004)].

18. J. B. Goodenough, H. Y.-P. Hong, and J.A. Kafalas, Mater. Res. Bull. **11**, 203 (1976).

19. E. Breval, H. A. McKinstry, and D. K. Agrawal, Brit. Ceram. Trans. **93** (6), 239 (1994).

20. A. Martínez-Juárez, J. E. Iglesias, and J. M. Rojo, Solid State Ionics **91** (3–4), 295 (1996).

21. V. I. Pet'kov, A. N. Loshkarev, A. I. Orlova, et al., Zh. Neorg. Khim. **47** (7), 1162 (2002) [Russ. J. Inorg. Chem. **47** (7), 1053 (2002)].

22. V. I. Pet'kov, A. I. Orlova, I. G. Trubach, et al., Czech. J. Phys. **53**, A639 (2003).

23. H. M. Rietveld, Acta Crystallogr. **22**, 151 (1967).

24. Y. I. Kim and F. Izumi, J. Ceram. Soc. Jpn. **102**, 401 (1994).

25. F. Izumi, *The Rietveld Method*, Ed. by R. A. Ch. Young (Oxford Univ. Press, New York, 1993).

26. S. Yu. Stefanovich, *Proceedings of the European Conference on Lasers and Electro-Optics (OLEO-Europe 94), Amsterdam, 1994* (Amsterdam, 1994), p. 249.

27. R. G. Sizova, V. A. Blinov, A. A. Voronkov, et al., Kristallografiya **26** (2), 293 (1981).

28. V. I. Pet'kov, G. I. Dorokhova, and A. I. Orlova, Kristallografiya **46** (1), 76 (2001) [Crystallogr. Rep. **46** (1), 69 (2001)].